Signature of a West Wind Convective Event in SSM/I Data

John Joseph BATES

Climate Research Division, NOAA/ERL
325 Broadway
Boulder, CO 80303 - U.S.A.

1. Introduction.

In the western equatorial Pacific, the net heat flux into the ocean is approximately a balance between heat input due to solar flux and heat loss due to evaporative cooling. Climatologies such as Weare et al. (1981) show the region west of the dateline from 10°N to 10°S to be an area of net oceanic surface heating of from 30-60 W m^{-2}. Although much smaller in magnitude than the short-wave and latent heat fluxes, the longwave and sensible heat fluxes can not be ignored, since the net flux is so small. The largest discrepancies between climatologies of net heat flux in the western equatorial Pacific [e.g., between Weare et al. (1981) and Wyrtki (1965)] occur in the estimation of the latent heat flux.

Work by Meyers et al. (1986) has shown that anomalous cooling of the ocean upper mixed layer during the 1982-83 ENSO episode was caused primarily by anomalous evaporative cooling. Their work was confined, however, to a rather limited spatial domain (i.e., 2°S-4°N and 150-170°E). Since the location of deep convection, and the teleconnections to the mid-latitudes that can result in regional short-term climate anomalies, are highly correlated to equatorial sea surface temperature, it is important to monitor the larger temporal and spatial patterns associated with evaporative cooling anomalies. Remote sensing is one means of obtaining the coverage necessary to adequately monitor evaporative cooling anomalies.

2. Remote sensing of moisture and wind speed using SSM/I.

The Special Sensor Microwave Imager (SSM/I) on the Defense Meteorological Satellite Program (DMSP) polar-orbiting spacecraft has been operating since July 1987. Similar instruments are planned to fly on all future DMSP spacecraft, offering the possibility of two SSM/I instruments covering the earth in the future. SSM/I scans at four frequencies; 19, 22, 37 and 85 GHz as well as dual polarizations except at 22 GHz (Hollinger et al., 1987). The SSM/I provides improved coverage, spatial resolution, and accuracy over prior passive microwave intruments, but lacks the lower frequency channels that allow sea surface temperature to be retrieved.

The 22 GHz channel is primarily used for estimating integrated water vapor content, since it is located near the center of a weak water vapor absorption line. Dr. J. Alishouse, NESDIS, has performed a statistical regression of co-located radiosonde estimates of integrated water vapor with observed SSM/I brightness temperatures (Alishouse et al., 1989). These statistical results, as well as theoretical results, show that the SSM/I 22 GHz channel has less sensitivity to high moisture concentrations due to a nonlinear relation between moisture and the 22 GHz brightness temperature. This has important consequences for remote sensing of moisture in the TOGA COARE region. For example, using Alishouse et al. (1989) tropical nonlinear algorithm, the error in retrieving moisture due to noise in the 22 GHz channel alone is only 0.6 kg m^{-2} in a

typical subtropical atmosphere, while it is 1.22 kg m^{-2} for a moist tropical atmosphere. The actual retrieval error is larger since additional channels are used in the regression to account for attenuation in the atmosphere and emission from the sea surface.

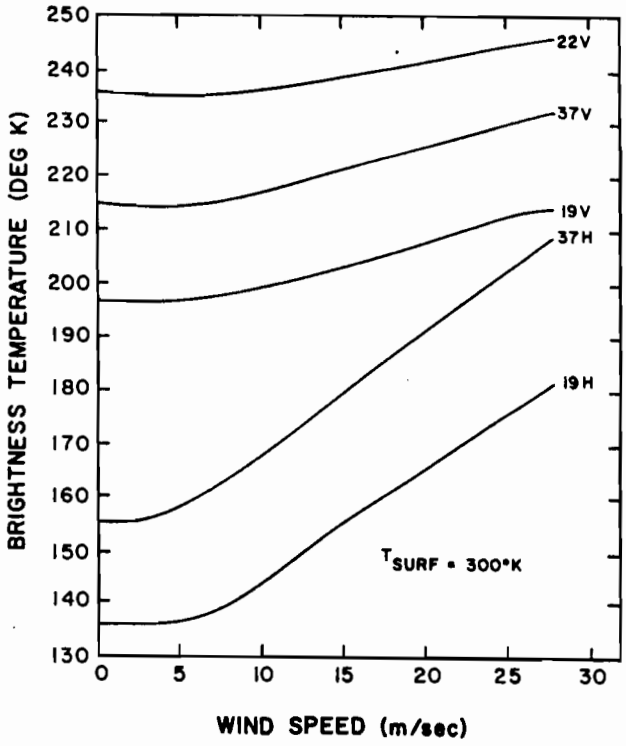

FIG.1. SSM/I brightness temperature as a function of frequency and wind speed.

The physical basis for estimating wind speed from passive microwave data is illustrated in Figure 1. At the SSM/I incidence angle (approximately 54°), vertically and horizontally polarized microwave radiation have a differential sensitivity to wind roughening of the sea surface. The sensitivity is greatest for the 37 GHz channels. The effect on the 37 GHz channels, however, is not apparent until wind speeds are in excess of 3 m s^{-1}. This is important to TOGA COARE since some regions of the equatorial western Pacific have mean wind speeds less than 3 m s^{-1}. It may be possible to classify these low wind speed regions by identifying unique signatures of SSM/I brightness temperature profiles, but this has yet to be shown. Fortunately, we are interested in anomalously large evaporative cooling events for which wind speeds should be great enough for SSM/I to detect. We are using the revised statistical wind speed algorithm of Goodberlet (1989) which was derived from regression of buoy wind speed observations against co-located SSM/I brightness temperature observations.

SSM/I estimates of both integrated water vapor content and surface wind speed are degraded in the presence of large cloud water droplets (>100 microns) and precipitation. Thresholds on the 19 GHz horizontally-polarizeed channel brightness temperature and the difference 37V-37H channel brightness temperatures are used to screen for such conditions. For this study, we have required that 19H < 185 K and that 37V-37H and that 37V-37H > 50 K.

Sixty days of SSM/I data, from mid-January through mid-March 1988, over the western equatorial Pacific has been extracted, calibrated, and geo-located. Goe-locations have been adjusted to agree with know landmarks using a correction algorithm provided

by Dr. C. Swift. The data have also been quality controlled using reasonable bounds on the derived brightness temperatures. The data were binned on a 50 km by 50 km grid daily with only the single most recent sample in the bin being saved. Land areas and areas with no retrievals, due to exceeding the cloud thresholds for all five days, are left blank. The daily and five-day (pentad) average binned data were objectively analyzed using a Barnes two-pass scheme on a 100 km by 100 km grid to produce the contour maps shown.

3. Case study.

Using Outgoing Longwave Radiation (OLR) data, several convective events were found during winter 1987-88 propagating eastward from the Indian Ocean through the Indonesian area and into the western equatorial Pacific. These events were identified as 5-day mean OLR values of less than 200 W m^{-2} (Figure 2) and negative OLR anomaly values of less than 20 W m^{-2}. NMC 850 mb wind analyses showed that westerly winds were associated with the movement of a convective event in late February, with peak wind speeds of up to 15 m s^{-1} located off the northeastern tip of Australia during the pentad of February 20-24. COADs ship data, however, did not show such a dramatic wind burst. SSM/I data were analyzed for the 60-day period in an attempt to capture the characteristics of this event in passive microwave data.

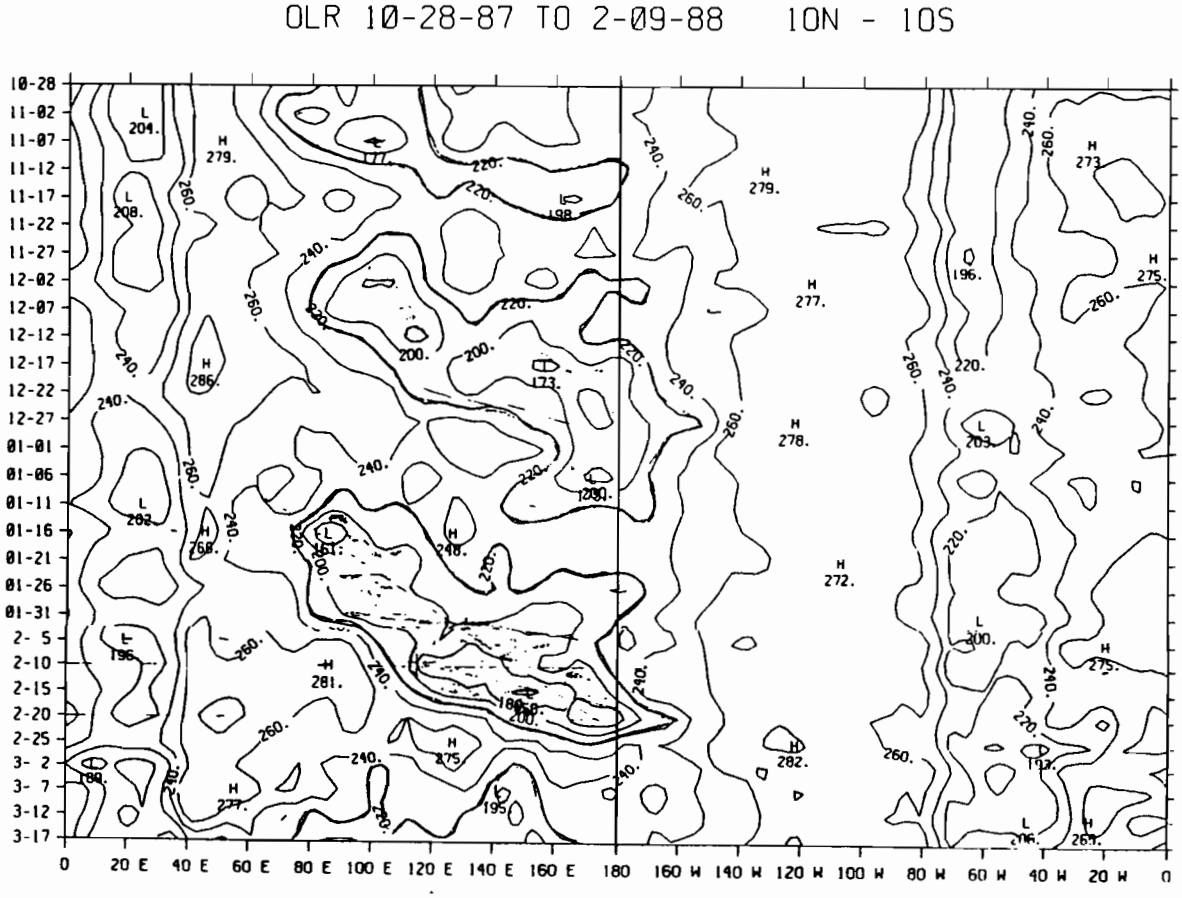

FIG.2. Time-longitude section of outgoing longwave radiation (OLR).

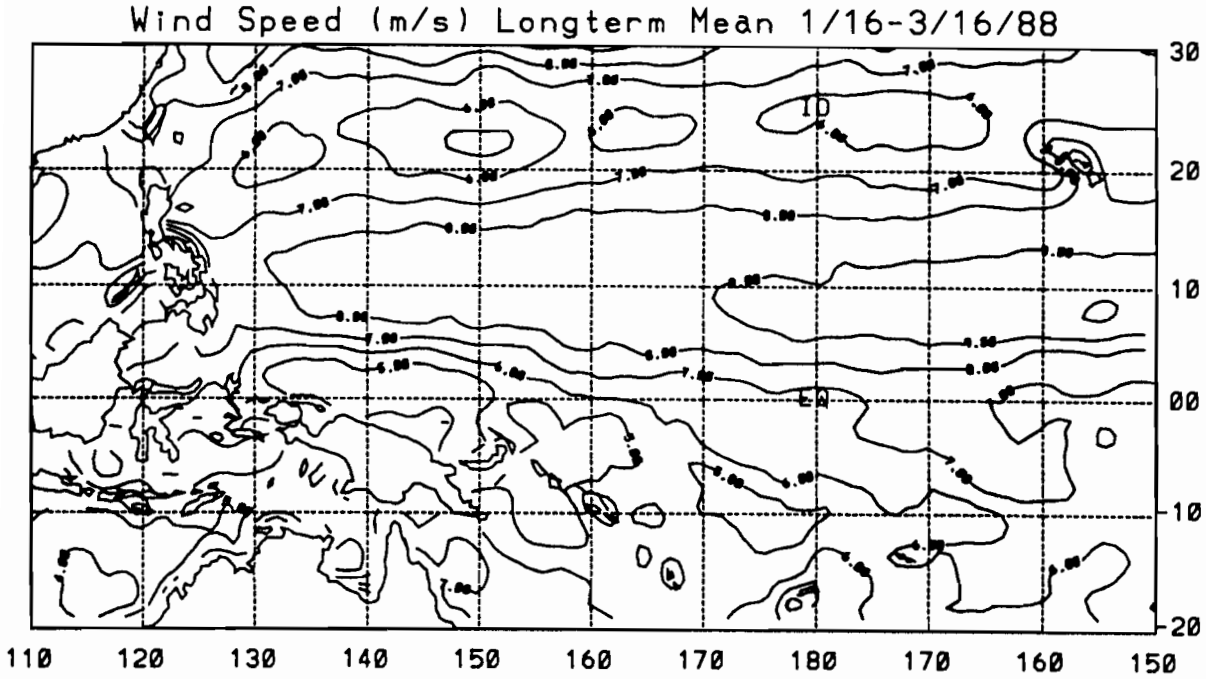

FIG.3. Long-term mean (14 January-14 March 1988) wind speed (m s^{-1}) from SSM/I.

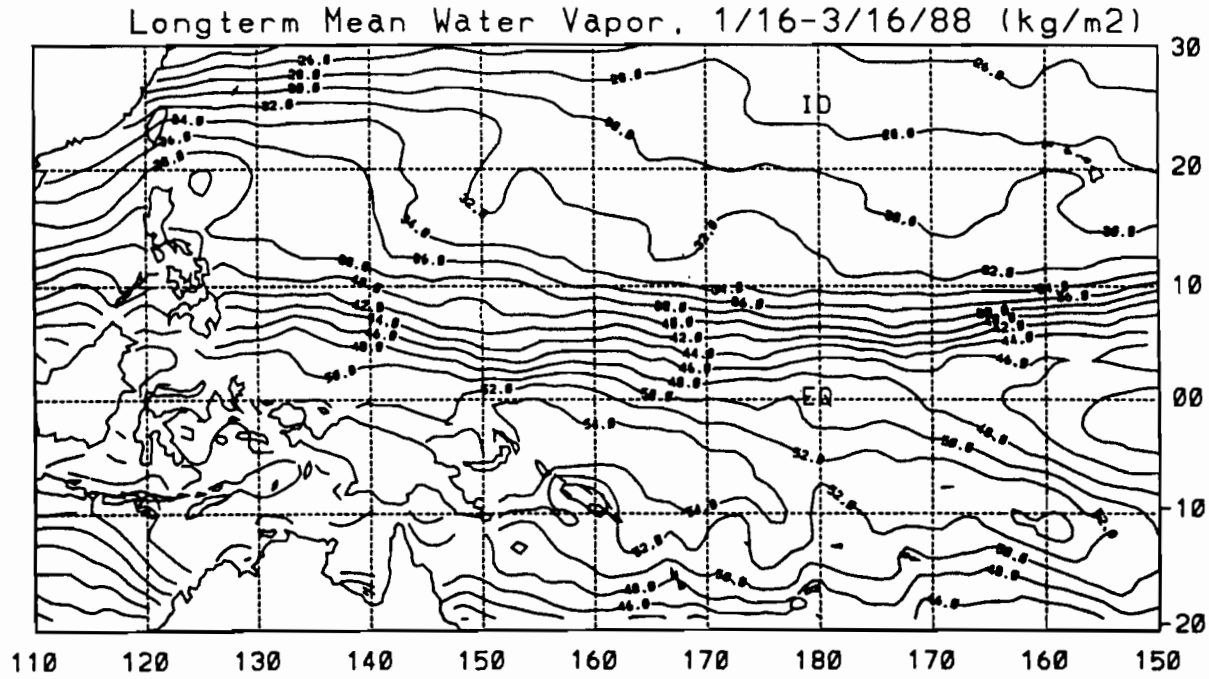

FIG.4. Long-term mean (14 January-14 March 1988) total precipitable water (kg m^{-2}) from SSM/I.

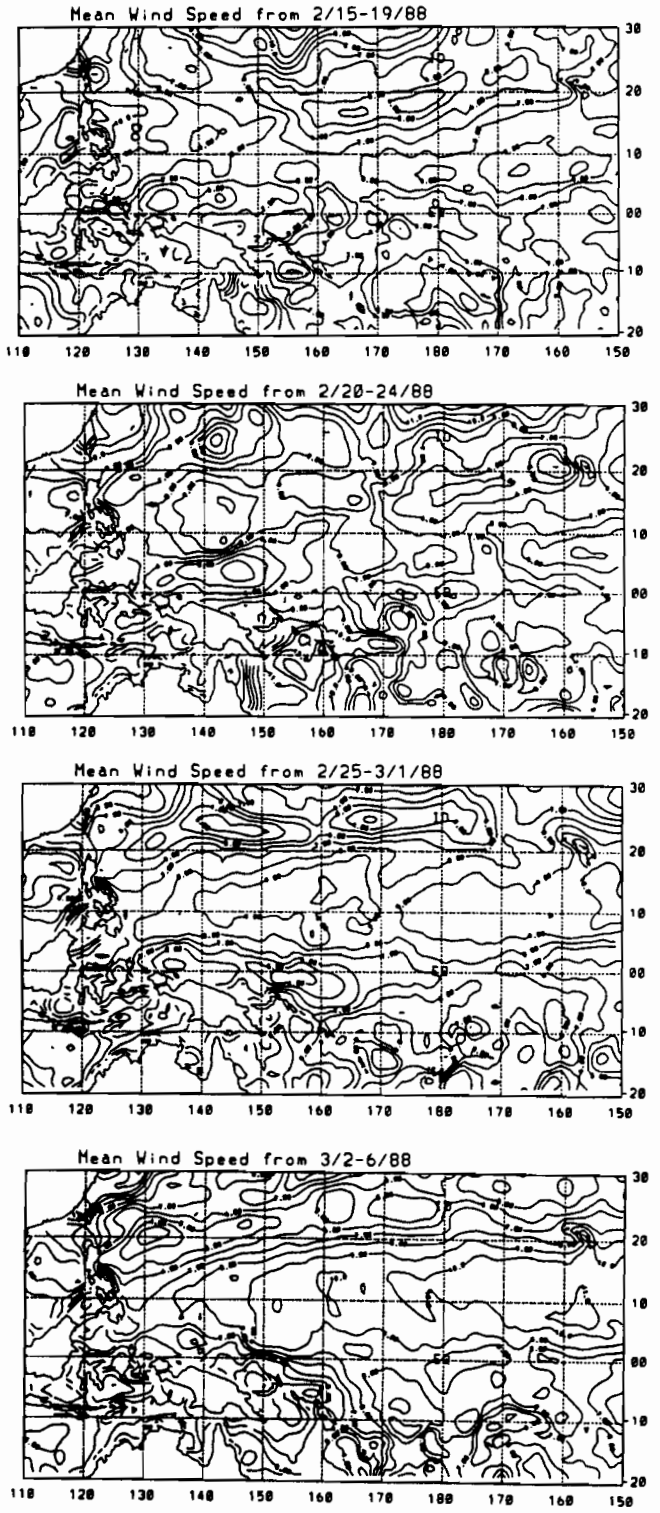

FIG.5. Pentads (5-day means) of wind speed (m s^{-1}) and total precipitable water (Kg m^{-2}) from SSM/I.

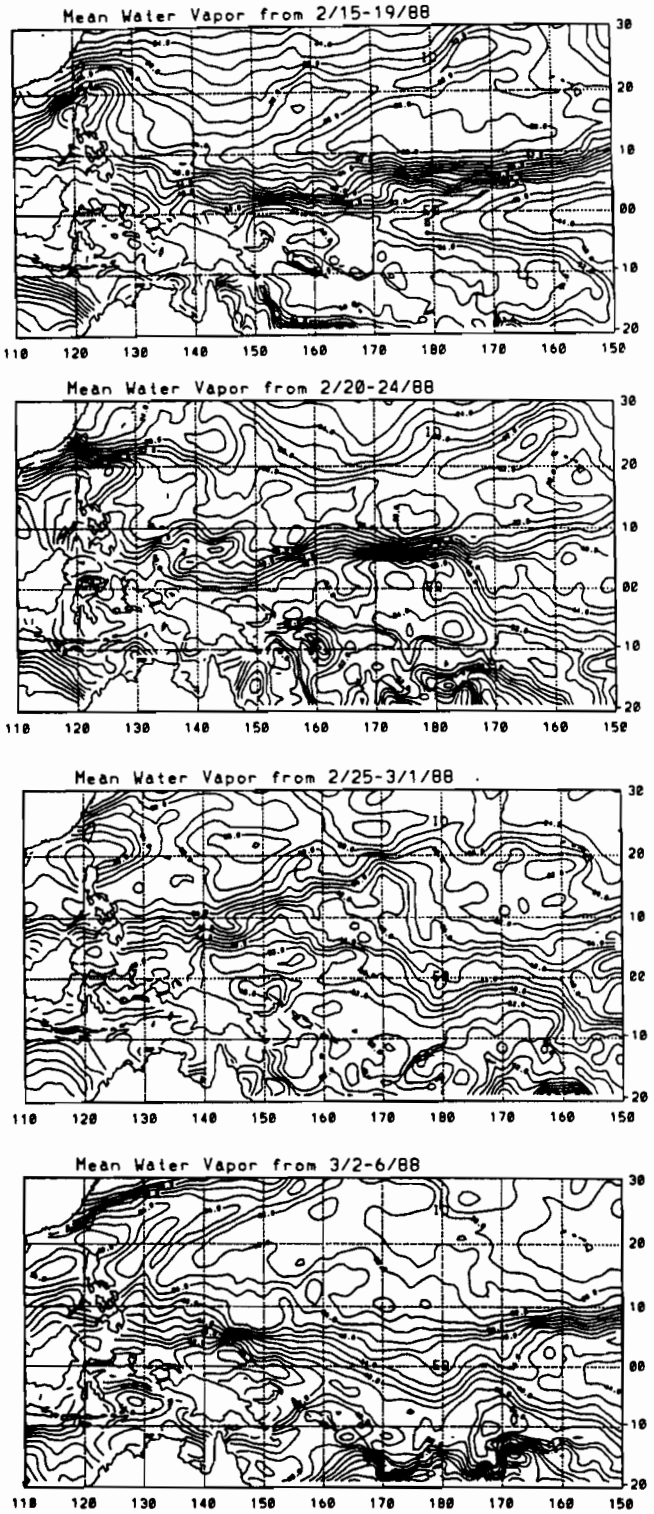

FIG.5. (Continue)

The long-term mean analysis of wind speed derived from SSM/I data (Figure 3) shows a band of high wind speeds along 30°N, extending south along the coast of southeast China toward the Philippines. A band of lower wind speeds is found along 20°N, while a broad zone of high wind speeds extends from 15°N to 5°N. A crescent-shaped region of low wind speeds is seen around Australia. The long-term mean integrated water vapor analysis (figure 4) shows a maximum along and south of the equator with a split into the ITCZ and SPCZ in the eastern edge of the domain. Low values of integrated water vapor are found north of 20°N.

Pentads of wind speed and integrated water vapor imagery, the objective analyses, and the objective analyses of anomalies from the long-term mean are shown in Figure 5. The wind speed analyses show a high degree of spatial variability. The first clear evidence of increased wind speeds associated with the convective event is found in the pentad of February 15-19 off northeastern Australia. In the following pentad, very high winds are found surrounding an area blacked out due to persistent precipitation during the five-day period. Wind speeds in this area are in excess of 11 m s^{-1}. High wind speeds, but not as dramatic, propagate to the east in association with the convective event in the next two pentads. Throughout this 60-day period, the moisture field undergoes a large oscillation. Prior to the convective event, large amounts of integrated water vapor are found associated with the convective region over the western Pacific warm water pool. At the height of and following the passage of the convective event, dramatically less amounts of integrated water vapor are found over the equatorial region.

In order to better quantify the standing oscillation patterns, principal component analysis has been used to examine the daily objectively analyzed fields of wind speed, integrated water vapor, and a latent flux parameter (the wind speed multiplied by the integrated water vapor concentration). Only the first principal component from each variable is shown, and in each case this component is significantly different from random noise at the 95% confidence interval.

The spatial pattern of the first EOF of wind speed (Figure 6) shows positive centers of action located from 10°N to 20°N and 160°E to 190°E and south of the equator from 160°E to 200°E. Negative centers cover much less area and occur off the coast of southeast Asia and near 10°N, 120°E. The amplitude time series that modifies this spatial pattern shows several oscillations over the sixty day period, with the highest values being positive from days 55-65. This corresponds to the time of passage of the west wind burst.

The first EOF integrated water vapor spatial pattern (Figure 7) shows a maxima center of action along the equator, extending north along the Phillipines, and curving back to the east along 20°N. Negative centers are found off the coast of southeast Asia and near 15°N, 160°E. The associated amplitude time series shows an extreme negative excursion between days 50-60, slightly leading the maxima in the wind speed EOF.

In a first attempt at inferring the latent heat flux from these data, an EOF analysis was performed on the flux parameter wind speed times the integrated water vapor content. This field was not standardized prior to calculating the EOF; standardizing does not significantly change the results. Centers of action (Figure 8) are located in two zonal bands; one from 10°N-20°N, the other 5°S-15°S. Positive centers are found between 120°E-140°E, and negative centers are found between 150°E-200°E. the largest amplitudes are reached between days 53-63. This indicates enhanced positive values of the flux parameter in the region of the convective event during the time of its passage. There also seems to be a symmetric response in the northern hemisphere, although the convective event was largely confined to the southern hemisphere.

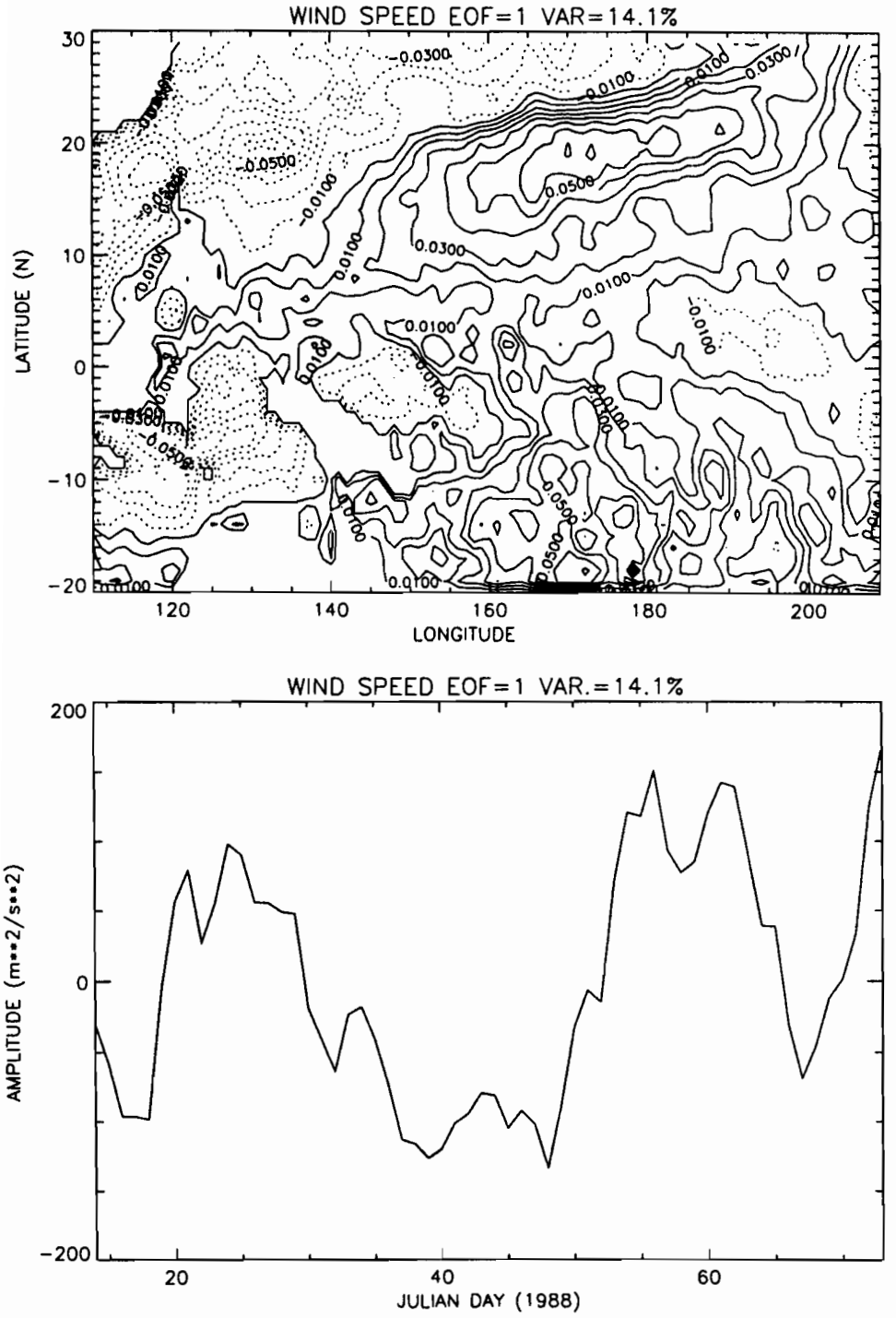

FIG.6. First EOF of SSM/I daily wind speeds.

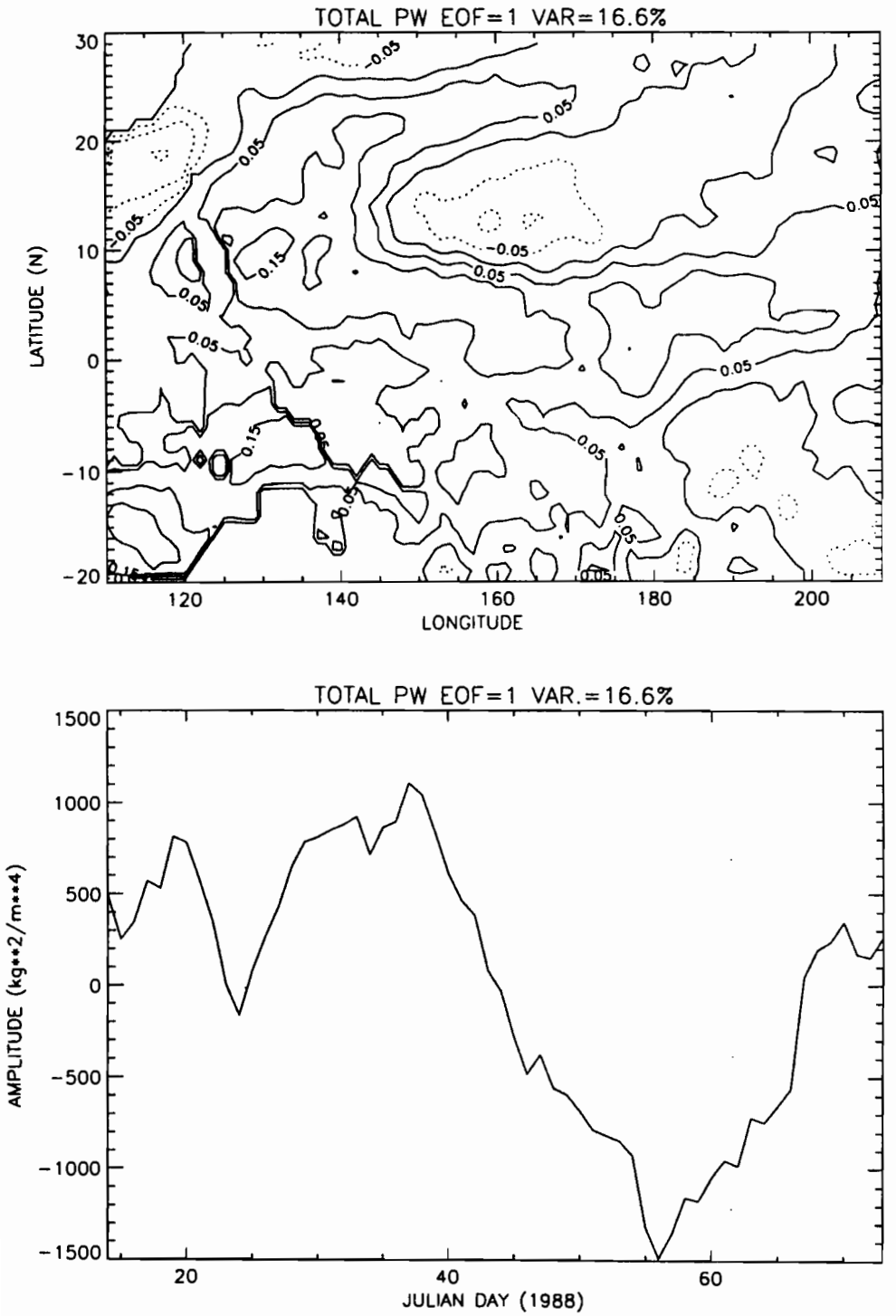

FIG.7. First EOF of SSM/I daily total precipitable water.

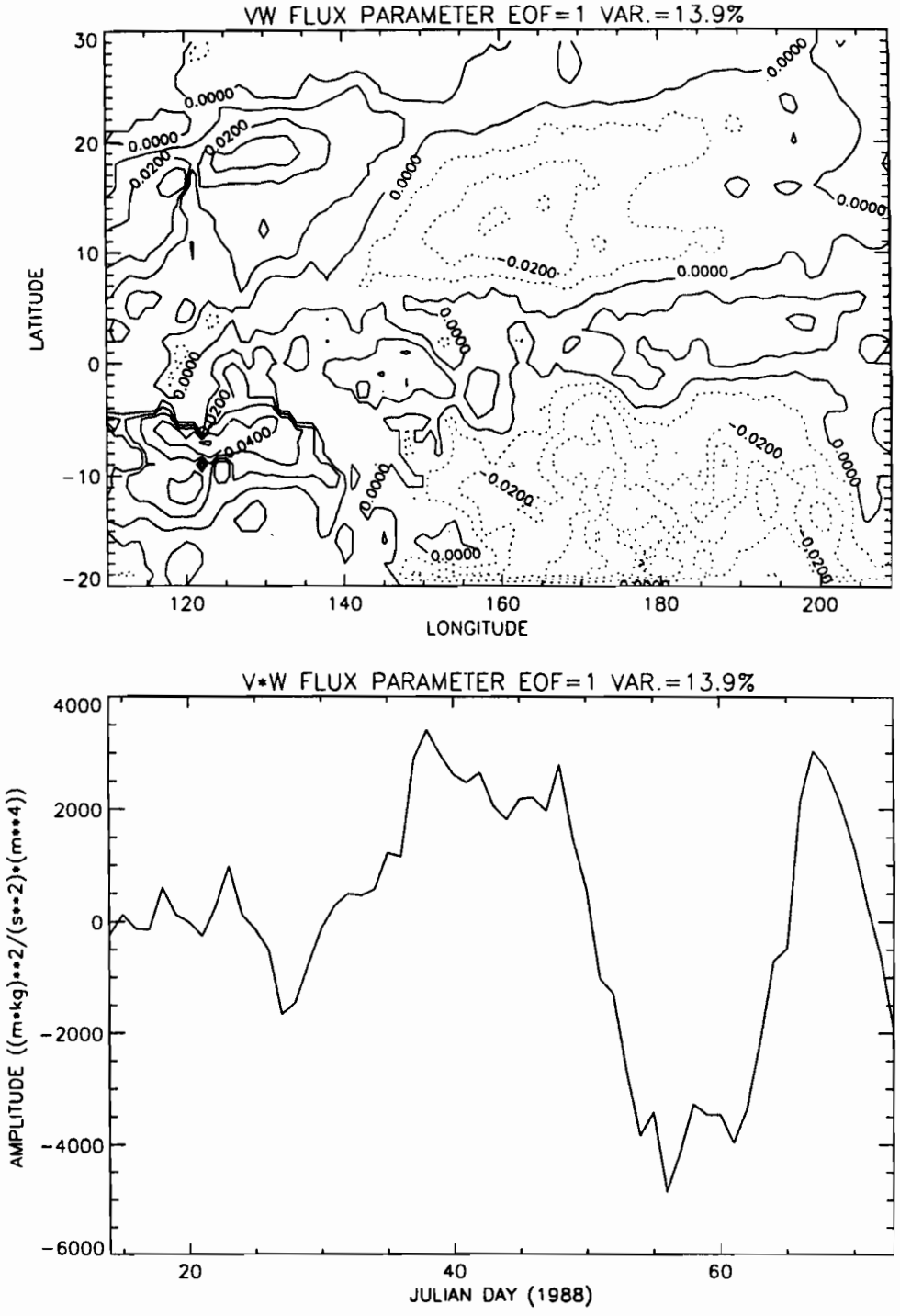

FIG.8. First EOF of SSM/I flux parameter.

4. Continuing work and TOGA COARE pilot studies.

The objective of this work is to analyze moisture and latent heat flux variability starting with a case study of a single convective event, but eventually we hope to extend the analysis to the entire tropical oceans, using a method similar to Liu (1988). While the improved accuracy and coverage of data provided by the SSM/I hold great promise, several significant roadblocks remain. First, to estimate the latent heat flux on daily or weekly time scales, a relationship between integrated water vapor content and surface specific humidity, similar to that of Liu (1986) for monthly time scales, must be established for the shorter time scales. Second, we must find a parameterization for the latent heat flux in disturbed, convective regimes where precipitation interferes with microwave observations of wind speed and integrated water vapor. Finally, since SSM/I does not contain low frequency microwave channels, we must rely on other remote sensing and *in situ* observations of sea surface temperature. We are continuing to work on all theses issues.

I would hope that this work could be continued as part of a pilot study of moisture and latent heat flux variability over the TOGA COARE region. For such a study, the region should be expanded longitudinally in both directions to include all of the Pacific and Indian oceans. The Indian ocean has been identified as being intimately connected to atmospheric oscillations in the western equatorial Pacific.

Acknowledgments. This research has been funded by the Equatorial Pacific ocean Climate Studies (EPOCS) program. Drs. C. Swift and J. Alishouse kindly provided their updated algorithms for retrieval of wind speed and integrated water vapor from SSM/I data.

REFERENCES

Alishouse, J.C., S. Snyder, and J. Vongsathorn, 1989: Determinations of total precipitable water in the tropics from the SSM/I. *Preprints Forth Conference on Satellite Meteorology and Oceanography,* San Diego, CA, .

Goodberlet, M., 1989: Remote sensing of ocean surface winds with the SSM/I, 1989: *Preprints Forth Conference on Satellite Meteorology and Oceanography,* San Diego, CA, .

Hollinger, J., R. Lo, G. Poe, R. Savage, and J. Peirce, 1987: *Special Sensor Microwavel/Imager User's Guide,* Naval Research Laboratory, Washington, D.C., 119 pp..

Liu, W.T., 1986: Statistical relation between monthly precipitable water and surface-level humidity over global oceans, *Mon. Weather Rev.*, **114**, 1591-1602.

Liu, W.T., 1988: Moisture and latent heat flux variabilities in the tropical Pacific derived from satellite data, *J. Geophys. Res.*, **93**, 6749-6760.

Meyers, G., J.R. Donguy, and R.K. Reed, 1986: Evaporative cooling of the western equatorial Pacific Ocean by anomalous winds, *Nature,* **323**, 523-526.

Weare, B.C., P.T. Strub and M.D. Samuel, 1981: Annual mean surface heat fluxes in the tropical Pacific Ocean, *J. Phys. Oceanogr.*, **11**, 705-717.

Wyrtki, K., 1965: The average annual heat balance of the North Pacific ocean and its relation to ocean circulation. *J. Geophys. Res.*, **70**, 4547-4559.

WESTERN PACIFIC INTERNATIONAL MEETING AND WORKSHOP ON TOGA COARE

Nouméa, New Caledonia
May 24-30, 1989

PROCEEDINGS

edited by

Joël Picaut *
Roger Lukas **
Thierry Delcroix *

* ORSTOM, Nouméa, New Caledonia
** JIMAR, University of Hawaii, U.S.A.

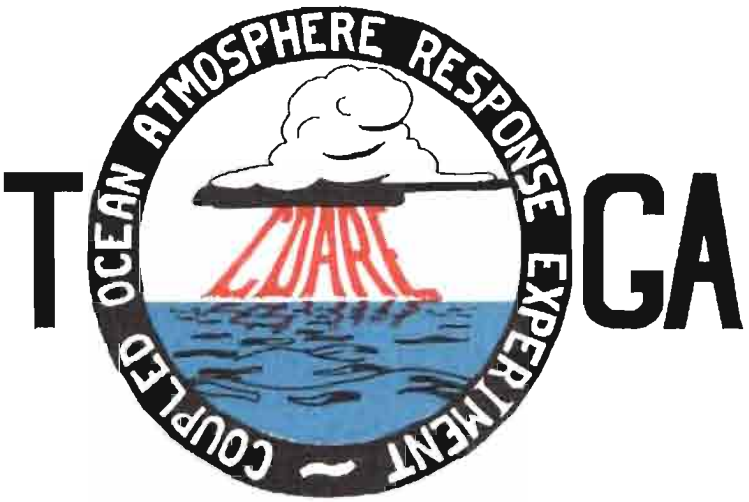

INSTITUT FRANÇAIS DE RECHERCHE SCIENTIFIQUE
POUR LE DÉVELOPPEMENT EN COOPÉRATION

ORSTOM

Centre de Nouméa

TABLE OF CONTENTS

MEETING COLLECTED PAPERS

WATER MASSES, SEA SURFACE TOPOGRAPHY, AND CIRCULATION

EL NINO/SOUTHERN OSCILLATION 1986-87

THEORETICAL AND MODELING STUDIES OF ENSO AND RELATED PROCESSES

MOMENTUM, HEAT, AND MOISTURE FLUXES BETWEEN ATMOSPHERE AND OCEAN

EMPIRICAL STUDIES OF ENSO AND SHORT-TERM CLIMATE VARIABILITY